




# BOREHOLE EFFECTS ON COAXIAL AND COPLANAR LOGS OF TRIAXIAL TOOLS IN LAMINATED FORMATIONS WITH ANISOTROPIC SHALE HOST

Paulo Roberto de Carvalho <sup>1\*</sup>, Cícero Régis <sup>2,3</sup>,  
and Valdelírio da Silva e Silva <sup>2</sup>

<sup>1</sup>Universidade Federal Rural da Amazônia - UFRA, Belém, PA, Brazil

<sup>2</sup>Universidade Federal do Pará - UFPA, Belém, PA, Brazil

<sup>3</sup>Instituto Nacional de Ciência e Tecnologia de Geofísica do Petróleo - INCT-GP, Brazil

\*Corresponding author: [cicero@ufpa.br](mailto:cicero@ufpa.br)

**ABSTRACT.** This paper studies the borehole effect in the triaxial induction logs within sand-shale laminated models with isotropic and anisotropic shale laminae with transverse isotropy. This study compares results from a 3D Vector Finite Element program (with borehole) and a 1D-Analytic code (no borehole). In comparison with the coaxial configuration, the vertical coplanar logs show a stronger honing effect in front of the laminated pack boundaries; a stronger skin effect to the conductivity media; and a more prominent oscillation within the laminated formation. In addition, feature changes (angular or smooth shapes) occur on the coaxial and coplanar responses as the dipping angle varies. The sensitivities of the logs to the anisotropy and borehole are opposite, i.e., for small angles where the coaxial is least sensitive, the coplanar is most sensitive, and for large angles where the coaxial is most sensitive, the coplanar is least sensitive. The main physical cause of these opposite behaviors to the anisotropy and borehole effect is the same: the weight of the horizontal magnetic component of the horizontal dipole contribution on the coaxial and coplanar dipping logs since it is the only one of the four magnetic field components that has anisotropy sensitivity and strongest skin effect.

**Keywords:** Borehole effects, triaxial induction tool, laminated sand-shale formations, electrical anisotropy, anisotropic shale host

## INTRODUCTION

The deepwater turbidite reservoirs from Campos Basin comprise one of Brazil's most important offshore petroleum accumulations. These reservoirs can be very complex and heterogeneous, ranging from massive thick sands to highly laminated sand-shale sequences. A laminated reservoir, as illustrated in figure 1, consists of thin layers alternating between conductive water-bearing shales and resistive oil-bearing sands (Gomes et al., 2002).

Thinly laminated reservoirs are described by a typical effective electrical anisotropy because the single layers cannot be individually resolved by the resistivity induction tools. The horizontal conductivity,  $\sigma_h$ , parallel to the layers is more strongly controlled by the shale, whereas the vertical conductivity,  $\sigma_v$ , perpendicular to the layers, is dominated by the resis-

tive hydrocarbon sand zones. This type of anisotropy is usually referred to as structural or macroscopic anisotropy.

From the beginning of this century, the need for more information from interbedded sand-shale turbidite sequences prompted the development of the triaxial or multicomponent wireline induction tool, with nine coupling components, that have been successfully used to determine formation anisotropy and bedding dip angle (Kriegshäuser et al., 2000). Currently, besides being the main location tool of finely laminated reservoirs, triaxial sources and sensors are also applied in many situations of asymmetric geometry, such as locating dissolution cavities (vugs) in carbonates and fractured zones in the vicinity of the wells, and monitoring invasion fronts in horizontal wells (Omeragic et al., 2015).

Over the past ten years, new configurations have appeared that use real-time transmission of the nine components to allow inversion methods to determine both resistivity and anisotropy, as well as the dip angle and azimuth of the formation. For example, an electromagnetic azimuthal resistivity logging while drilling (EM-LWD) tool (Clegg et al., 2021), and a higher frequency Electromagnetic Look-Ahead (EMLA) tool (Bittar et al., 2021), have been used to enable proactive geosteering and reservoir mapping, investigating several meters away from the borehole and ahead of the drill-bit.

The simplest multicomponent triaxial induction tool consists of three mutually orthogonal coil transmitters and receivers. Figure 1 illustrates two of the nine possible transmitter-receiver combinations in a borehole with diameter  $D$ : the coaxial configuration, where the dipole moment of the source and the receiver are aligned with the tool axis, and a coplanar configuration with the dipole moment of the source normal to the axis in the  $(x, z)$  plane.

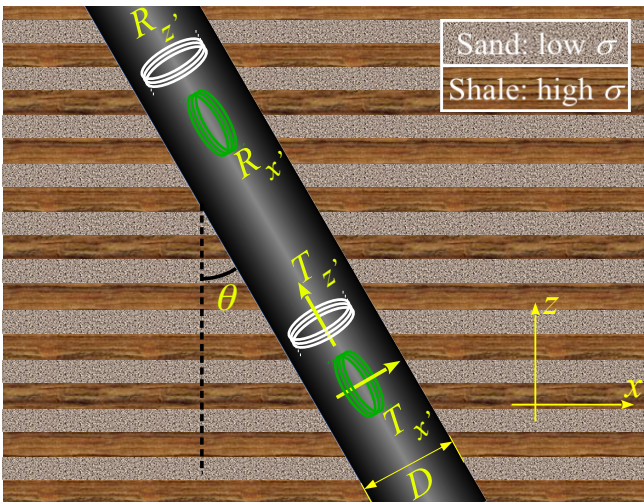


Figure 1: Laminated sand-shale sequence and illustration of the transmitters and receivers of the coaxial and coplanar coil configurations.

The profiles presented here will be in straight boreholes positioned in the  $(x, z)$  plane, and only the coaxial ( $z'$  direction) and coplanar ( $x'$  direction) configurations will be simulated. Using the coordinate system illustrated in figure 1, in both 1D and 3D cases the observed magnetic fields at the receiver coils for the coaxial ( $H_{z'z'}$ ) and coplanar ( $H_{x'x'}$ ) configurations with source dipole moments  $m_{x'} = m_{z'} = m$  are the combination of four signals: the vertical ( $H_{zz}$  and  $H_{xz}$ ) and horizontal ( $H_{zx}$  and  $H_{xx}$ ) components from the vertical (VMD) and horizontal (HMD) dipole sources. These are the ones needed to simulate the responses at any dip angle  $\theta$  measured in relation to

the vertical  $z$ -axis:

$$H_{z'z'} = m [H_{xx} \sin^2 \theta + (H_{xz} + H_{zx}) \sin \theta \cos \theta + H_{zz} \cos^2 \theta], \quad (1)$$

$$H_{x'x'} = m [H_{xx} \cos^2 \theta - (H_{xz} + H_{zx}) \sin \theta \cos \theta + H_{zz} \sin^2 \theta]. \quad (2)$$

The sensitivities of the coaxial ( $H_{z'z'}$ ) and coplanar ( $H_{x'x'}$ ) dipping logs to the anisotropy and borehole effect are opposite, i.e., for small dip angles where the coaxial is least sensitive to these effects, the coplanar is most sensitive, and for large dip angles where the coaxial is most sensitive, the coplanar is least sensitive. The main cause of these opposite behaviors is the relative weight of the contribution of the horizontal magnetic component of the horizontal dipole ( $H_{xx}$ ) to the coaxial ( $\sin^2 \theta$ ) and coplanar ( $\cos^2 \theta$ ) responses (equations 1 and 2), since that is the only one of the four magnetic field components that has anisotropy sensitivity (Kaufman and Ytskovich, 2017) and also the one that is subject to the strongest skin effect (Anderson et al., 2002).

Transversely isotropic (TI) homogeneous media have the same resistivity in every direction in the bedding plane, but a different resistivity normal to it. TI anisotropy is a reasonable assumption based on normal depositional processes. For a TI medium with a vertical axis of symmetry (TIV), Kaufman and Ytskovich (2017) show that, in the low frequency range, the anisotropy ratio  $\lambda^2$  is

$$\lambda^2 = \frac{\sigma_h}{\sigma_v} \approx \frac{\text{Im}\{H_{zz}\}/H_{zz}^{(0)}}{\text{Im}\{H_{xx}\}/H_{xx}^{(0)}}, \quad \omega \rightarrow 0, \quad \text{or} \quad \frac{L}{\delta} \ll 1, \quad (3)$$

where  $\sigma_h$  and  $\sigma_v$  are the horizontal and vertical conductivities,  $L$  is the transmitter-receiver offset,  $H_{zz}^{(0)} = m_z/(2\pi L^3)$  and  $H_{xx}^{(0)} = m_x/(4\pi L^3)$  are the free space direct mutual coil coupling for the coaxial and coplanar arrays, respectively, with source dipole moments  $m_z$  and  $m_x$ , and  $\delta$  is the largest plane wave skin depth in the medium. Anderson et al. (2008) show that this anisotropy index is a useful measurement because it alerts the log analyst to look for potential laminated pay-reservoir.

Complex apparent conductivities may be calculated from the coaxial  $\sigma_a^{cx}$  and coplanar  $\sigma_a^{cp}$  coil configurations, assuming an infinite homogeneous isotropic medium (Zhang et al., 2012):

$$\sigma_a^{cx} = \sigma_R^{cx} + i\sigma_X^{cx} = i\frac{4\pi L}{\omega\mu} H_{zz}, \quad (4)$$

$$\sigma_a^{cp} = \sigma_R^{cp} + i\sigma_X^{cp} = i\frac{8\pi L}{\omega\mu} H_{xx}. \quad (5)$$

where  $i = \sqrt{-1}$ ,  $\omega = 2\pi f$  is the angular frequency,  $f$  is the linear frequency, and  $\mu$  is the magnetic permeability.

Following Moran and Kunz (1962), in analogy to the usage in AC circuit theory, the real parts  $\sigma_R^{cx}$  and  $\sigma_R^{cp}$  are named quadrature or resistive components and the imaginary parts  $\sigma_X^{cx}$  and  $\sigma_X^{cp}$  are the inphase or reactive components of the coaxial and coplanar complex apparent conductivities, respectively.

The coaxial and coplanar mutual coupling signals ( $H_{zz}^{(0)}$  and  $H_{xx}^{(0)}$ ) are part of the imaginary components of the complex conductivities and are several orders of magnitude greater than the formation signals. Actual field tools usually contain additional “bucking” coils to cancel these large mutual coupling signals. However, since it is straightforward to calculate them analytically and remove them computationally (Anderson et al., 2002) we do not model bucking coils. The imaginary parts of the apparent conductivity after subtraction of the direct coupling are denoted by  $\sigma_{XF}^{cx}$  and  $\sigma_{XF}^{cp}$ .

The effective horizontal ( $\sigma_h$ ) and vertical ( $\sigma_v$ ) conductivities of a sand-shale ( $\sigma_{sd}$  and  $\sigma_{sh}$ ) thinly laminated formation, when their laminae thicknesses are less than the tool’s vertical resolution, are obtained by weighted arithmetic and harmonic means, respectively:

$$\sigma_h = \sigma_{sd}V_{sd} + \sigma_{sh}V_{sh}, \quad (6)$$

$$\sigma_v = \left( \frac{V_{sd}}{\sigma_{sd}} + \frac{V_{sh}}{\sigma_{sh}} \right)^{-1}, \quad (7)$$

where the weights  $V_{sh}$  and  $V_{sd} = 1 - V_{sh}$  are the volume fractions of each material, with  $V_{sh}$  obtained, for example, by spectroscopy probe (Anderson et al., 2008).

Equation 6 explains the strong dependence of  $\sigma_h$  on the shale laminae (high conductivity) and its poor sensitivity to the oil-bearing sand laminae (low conductivity).

Thus, sand laminae conductivity in vertical wells can be estimated from the horizontal (coaxial signal) and vertical (coplanar signal) apparent conductivities and applied in the classical Waxman and Smits (1968) model to estimate the water saturation in oil-bearing shaly sand reservoirs.

Originally, this method (Eqs. 6 and 7) assumed sand and shale laminae were isotropic. Laboratory measurements and field test results of the triaxial induction tool, however, showed that shale formations often exhibit conductivity anisotropy ( $\lambda^2 = 1$  to 8), originating from their micro-bedding structure with dimensions well below measurement resolution. Thus, in shales this type of anisotropy is a function of the compaction (clay porosity). This is usually referred to as intrinsic or microscopic anisotropy, and it is usually weaker than the structural anisotropy in laminated formations. Clavaud et al. (2005) show that intrinsic shale anisotropy plays an important role in the inversion of  $\sigma_v$  and  $\sigma_h$  data and, consequently, in the water saturation estimation of the finely laminated sand-shale reservoirs.

According to Moinfar et al. (2010) the borehole and the invasion zone effects on multi-component triaxial induction measurements can be significant, mainly in water-base muds. These effects may give rise to electrical pseudo-anisotropy in isotropic reservoirs with asymmetric invasion zones. Therefore, a quantitative assessment of the influence of the borehole on well logging data may contribute with important information to help in the borehole effect corrections and hence to improve the log interpretation.

To study the effect of the borehole, we have implemented a 3D Vector Finite Element program to simulate electromagnetic well logs in anisotropic formations. Using this program, we simulate well log data from vertical and dipping wells using both coaxial and coplanar coil configurations.

Here we present the results of a comparative analysis of the TIV-anisotropy level on the coaxial and coplanar responses in one-dimensional (no borehole) and three-dimensional laminated sand-shale models, with isotropic and anisotropic laminae, traversed by a borehole filled with a conductive water-based mud.

## THEORY AND ANALYSIS METHOD

The layered 1D problem is formulated using the mathematical tools described by Kaufman and Ytskovich (2017), generalized by us to multi-layered TIV media. The solutions are written as integrals of the Hankel transform, which are evaluated numerically using the Quadrature With Extrapolation (QWE) method as presented by Key (2012). The basic difference between this solution and the one for the 1D isotropic problem that we had previously implemented (Carvalho et al., 2010) is the manner of recursively computing the transmission and reflection coefficients on the interfaces. For the isotropic case, explicit analytic expressions are written for these coefficients allowing the use of recurrence relations, whereas in the anisotropic problem all coefficients are numerically determined by the solution of a system of linear equations whose size is proportional to the number of layers in the model.

The 3D problem is solved with an implementation of the Vector Finite Element method, using a secondary magnetic field formulation and following the steps presented by Jim (2015). In this solution, the total field is written as the sum of two parts: the *primary* field, which is the one generated by the source in a background (“primary”) medium for which there is an analytical or semi-analytical solution, and the *secondary* field, defined as the difference between the total and primary fields. Among other advantages, this separation avoids the difficulties of representing the point dipole sources in the discretized medium.

In our approach, the dipole sources are in an infinite unlimited homogeneous isotropic medium with the same conductivity as the drilling mud that simulates the environment inside the borehole. This choice

for the primary medium means that the secondary media occupy all the space outside the borehole, so that the primary electric field needs to be calculated in a great number of points in the mesh. However it presents two important advantages: it will easily allow the simulation of different geometries for the borehole in future work and it results in the primary electric field being calculated using an extremely simple formula, with minimum computational effort. For example, assuming a magnetic dipole in the  $x$  direction and located at the origin of the reference system, the expression for the electric field at coordinates  $(x, y, z)$  is (Ward and Hohmann, 1987, p. 176)

$$\mathbf{E} = \frac{i\omega\mu m_x}{4\pi r^2} (ikr + 1)e^{-ikr} \left( \frac{z}{r}\mathbf{u}_y - \frac{y}{r}\mathbf{u}_z \right), \quad (8)$$

where  $k = \sqrt{-i\omega\mu(\sigma + i\omega\epsilon)}$  is the (frequency domain) wave number,  $\epsilon$  is the electrical permittivity,  $r = \sqrt{x^2 + y^2 + z^2}$ , and  $\mathbf{u}_y$  and  $\mathbf{u}_z$  are unit vectors.

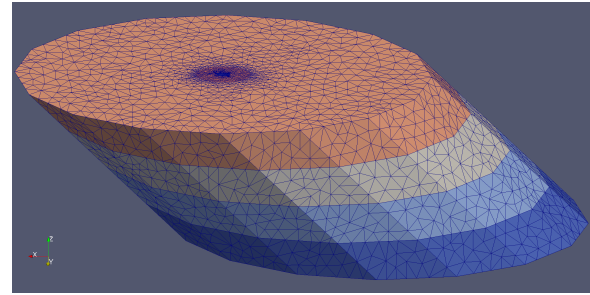
The problem is formulated to solve directly for the secondary magnetic field, which obviates the need to calculate numerical derivatives.

The system of linear equations generated by the Vector Finite Element method needs to be solved twice (once for each dipole) for every tool position in the profile, in all cases with the same complex sparse coefficient matrix. We chose to use the direct parallel solver PARDISO (Schenk et al., 2001) because a direct approach allows the factoring of the coefficient matrix only once, solving the multiple systems with only a phase of forward and backward substitutions each time. This means that the problem can be solved in shorter times than with an iterative solution. The software package PARDISO is implemented with an efficient memory management that stores only the non-zero elements of the matrix in every step of the factorization, which allows working with systems that would be simply impossible to fit in memory if the full matrix needed to be stored.

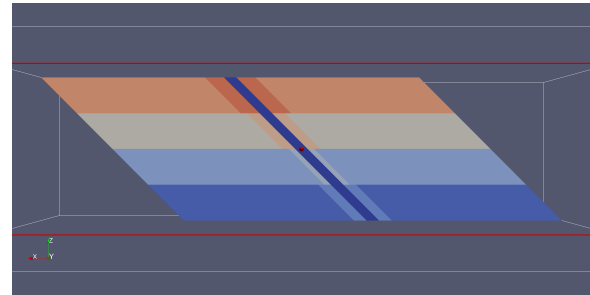
The 3D tetrahedral meshes were generated using the Tetgen software (Si, 2015). The mesh's outer boundaries are built following the cylindrical geometry of the well and invasion zones, as illustrated in figure 2. The radius from the well axis to the outer boundary of the mesh must be big enough to allow the application of homogeneous boundary conditions in the secondary magnetic field. The optimum radius depends on the frequency and range of resistivities in the model. In all results presented here a distance of 20 m from the dipole source was used.

## RESULTS AND DISCUSSIONS

In our simulations, the tool transmitters are magnetic point dipoles operating at 20 kHz and the source-receiver offset is  $L = 1.0$  m.



(a)



(b)

Figure 2: Illustration of the 3D tetrahedral mesh generated with Tetgen. Left: central part of the model, showing the cylindrical shape of the mesh's outer boundary. Right: vertical slice showing the central well and invasion zones.

According to Anderson et al. (1992) a laminated anisotropy level close to  $\lambda^2 = 2$  is a typical contrast for actual logging situations in laminated reservoirs. Therefore, in figures 3 to 5, the results are from a laminated formation containing low conductivity sands ( $\sigma_{sd} = 0.2$  S/m) alternating with high conductivity isotropic shales ( $\sigma_{sh} = 1.0$  S/m). Thicknesses of the sand and shale layers are equal and value 0.5 m ( $V_{sd} = V_{sh} = 50\%$ ). Thus, applying equations 6 and 7, the horizontal and vertical conductivities and the anisotropy ratio from an equivalent anisotropic bed are

$$\sigma_h = 0.6 \text{ S/m}, \quad \sigma_v = \frac{1}{3} \text{ S/m}, \quad \lambda_b^2 = \frac{\sigma_h}{\sigma_v} = 1.8. \quad (9)$$

Figure 3 shows a validation test with a comparison of the 3D and 1D logs for the laminated formation with the values listed in equation 9 in a dipping ( $60^\circ$ ) well. In this case, to simulate the measurements in the 3D code, the borehole diameter is made exceedingly small ( $D = 6$  cm) and the mud conductivity is equal to the geometric mean of the two laminae conductivities:  $\sigma_{md} = \sqrt{\sigma_{sh}\sigma_{sd}} = 1/\sqrt{5}$  S/m. In these conditions, it is expected that the borehole effects are small and the 1D and 3D solutions are similar.

The results show an excellent agreement between the 1D and 3D solutions within the laminated formation, except for a slight departure from the curves below and above the laminae package, where the conductivity contrast between the mud and the formation is greatest. This small effect appears on the resistive

logs, mainly on the coplanar signal, because of its well-known (Anderson et al., 2002) strongest skin effect (signal level attenuation and phase shift caused by the mud conductivity).

The resistive coplanar log is more sensitive to the laminae and shows a more prominent oscillation than the coaxial log. In addition, the so-called “polarization” horns are embedded in both coaxial and coplanar 1D and 3D results. These horns have been shown by Régis et al. (2020) to be associated with the discontinuous current density field parallel to the interfaces between layers, rather than with surface charge build-up from the continuous current across the interface, as was universally accepted since the early 1990s. They are unavoidable features of the coplanar profiles and are slightly smoothed by the influence of the well, a difference hard to notice for this very small diameter well, but more pronounced in regular wider wells, as shown in the next example.

These benchmarking results indicate a good validation between 1D and 3D responses, i.e., less than 1% difference inside the laminated formation. This gives us confidence in the accuracy for more complicated geometries.

A quantitative assessment of the influence of the borehole on well logging data may contribute with important information to help in interpretation. So, the goal going forward is to evaluate the percentage difference of the borehole effect on the 3D coaxial and coplanar signals in relation to those of the no-borehole 1D responses. For this, we compare the root mean square (RMS) of the signals in the middle of the laminated package in the depth range from -2.0 m to 2.0 m, i.e., away from the boundaries to the adjacent infinite shoulder beds above and below.

Figure 4 shows the 3D and 1D results for the same laminated formation as in the validation example, but now traversed vertically by a more realistic borehole with a 20 cm diameter, without invasion zones and filled with a water based 3 S/m mud.

First, notice within the laminated package a feature change on the resistive responses from the angular shape in figure 3 (dipping logs) to smooth shape in figure 4 (vertical logs). In the coaxial log, the curve becomes smooth because there is no contribution from any component in the transverse magnetic propagation mode with respect to the  $z$  direction ( $TM_z$ ) in the signal composition of the vertical component of the vertical dipole source. In the case of the coplanar log, the “horns” in the laminae interfaces, due to the  $TM_z$  mode influence (Régis et al., 2020) are smoothed out by the mutual canceling effect imposed by the multiple interface responses acting simultaneously. In addition, there is a curve reversal with respect to the model for both coaxial and coplanar resistive logs which stems from purely geometrical effects of the relative positions of the transmitter and the receiver within the laminae (Carvalho et al., 2018).

Comparing with an equivalent anisotropic bed

with conductivities calculated by equations 6 and 7, note that within the laminated formation the resistive coaxial signal oscillates closer to the horizontal  $\sigma_h = 0.6$  S/m, whereas the resistive coplanar signal oscillates closer to the vertical  $\sigma_v = 1/3$  S/m.

A much more pronounced borehole effect is observed on the resistive signals than on the deeper reactive signals for both coil arrays although this effect is visually greater in the coaxial reactive signal (7.6%) than on the coplanar reactive signal (-0.7%). As for the resistive signals, the borehole effect has the opposite behavior, i.e., the coaxial resistive signal increases (6.9%) whereas the coplanar resistive signal strongly reduces (-25.5%) due to the accentuated skin effect in this conductive mud.

Figure 5 shows the coaxial and coplanar deviated logs at  $60^\circ$  in the same laminated model as in figure 4. This dipping angle increases the borehole effect on the coaxial reactive (7.6% to 8.5%) and resistive (6.9% to 8.7%) signals, as compared to the vertical logs shown in figure 4. However, significant reductions are observed on the coplanar reactive (-0.7% to -0.02%) and resistive (-25.4% to -15.6%) signals.

The next examples show the 1D and 3D coaxial and coplanar vertical (figure 6) and dipping (figure 7) logs for a laminated formation analogous to the previous examples, but now the model has an anisotropic shale host ( $\lambda_{sh}^2 = 2$ ) with horizontal  $\sigma_h^{sh} = 1.0$  S/m and vertical  $\sigma_v^{sh} = 0.5$  S/m conductivities.

According to Clavaud et al. (2005) replacing  $\sigma_h^{sh}$  for  $\sigma^{sh}$  in equation 6 and  $\sigma_v^{sh}$  for  $\sigma^{sh}$  in equation 7 we obtain the anisotropic ratio from the equivalent anisotropic bed to this laminated formation with anisotropic shale laminae. Thus, the horizontal and vertical conductivities and the anisotropy ratio from an equivalent anisotropic bed to this new model are:  $\sigma_h = 0.6$  S/m,  $\sigma_v = 2/7$  S/m,  $\lambda_b^2 = \sigma_h/\sigma_v = 2.1$ . Therefore, due to the anisotropic shale laminae the anisotropy ratio is 17.7% greater than that of the previous isotropic laminae model ( $\lambda_b^2 = 1.8$ ).

In the vertical logs of figure 6 the coaxial signals are identical to those seen in figure 4, in which the shale laminae are isotropic. The percentage differences between 3D and 1D data on the coaxial reactive and resistive responses are exactly 7.6% and 6.9%, i.e., they are the same as in the isotropic case, because the coaxial vertical logs are insensitive to the vertical conductivity of the anisotropic shale laminae. However, these differences on the coplanar reactive and resistive data are -0.6% and -29.4%, respectively, whereas in the purely isotropic case (figure 4) they are -0.7% and -25.5%, respectively, due to the sensitivity of the coplanar configuration to the anisotropy of the shale laminae.

Now, in the dipping logs of figure 7, notice a new angular feature in the coaxial resistive responses due to the anisotropy of the shale laminae, whereas the coplanar responses have the same angular shape as seen in figure 5 for isotropic shale laminae. Again,

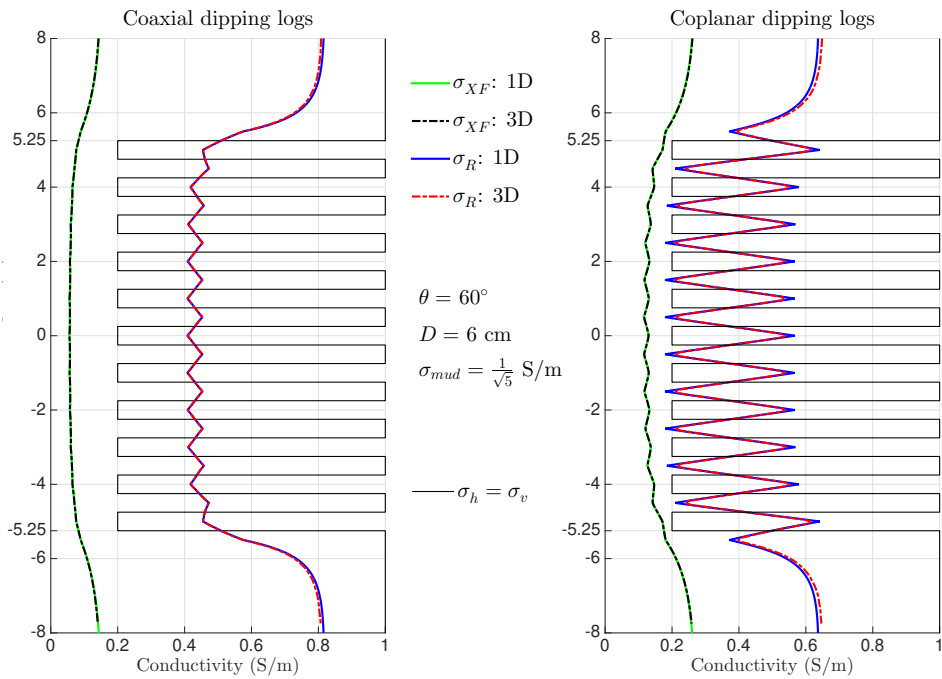


Figure 3: Validation test. Simulation of logs from a dipping well at  $60^\circ$ . 3D results generated with a very thin borehole with a 6 cm diameter and mud conductivity equal to the geometric mean of the two conductivities in the model.

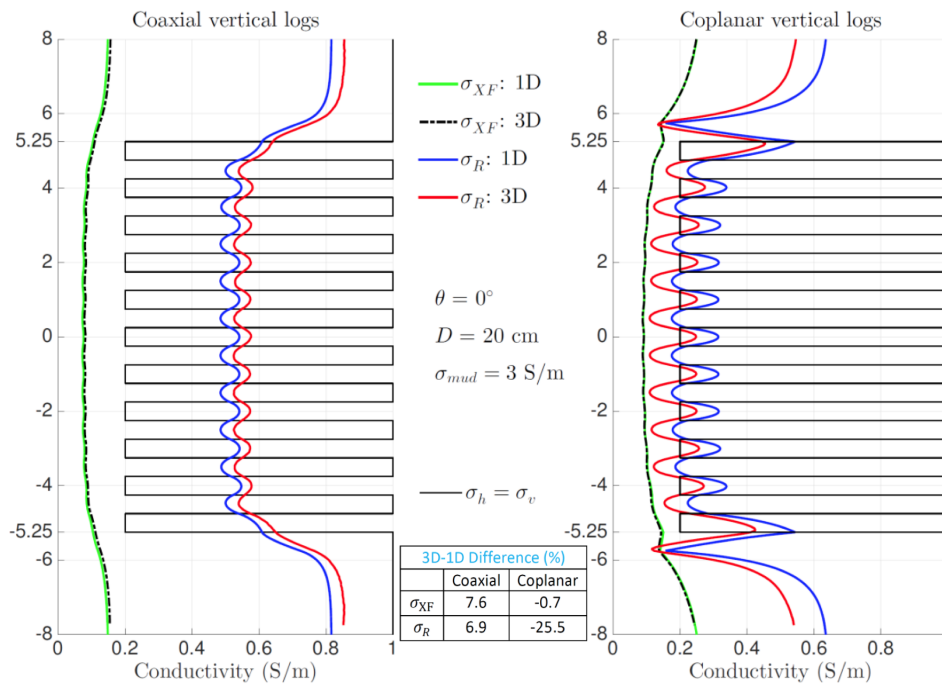


Figure 4: Comparison between logs without (1D) and with (3D) the influence of a borehole in a vertical well in an isotropic shale-sand laminated formation.

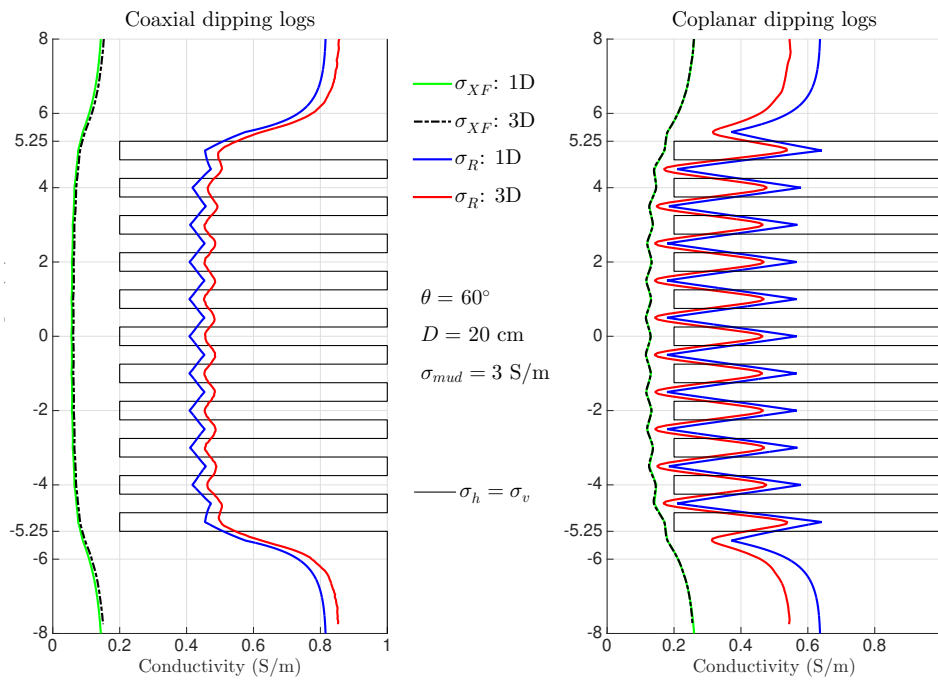


Figure 5: Comparison between logs without (1D) and with (3D) the influence of a borehole in a dipping well at  $60^\circ$  in an isotropic shale-sand laminated formation.

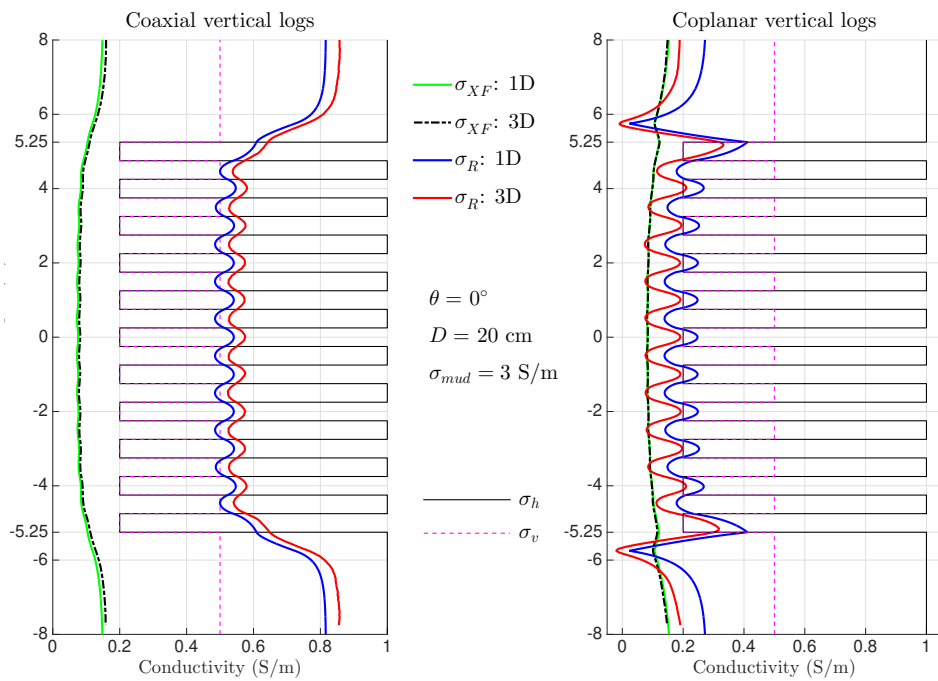


Figure 6: Comparison between logs without (1D) and with (3D) the influence of a borehole in a vertical well in a model composed of a sequence of isotropic sand laminae in an anisotropic shale host.

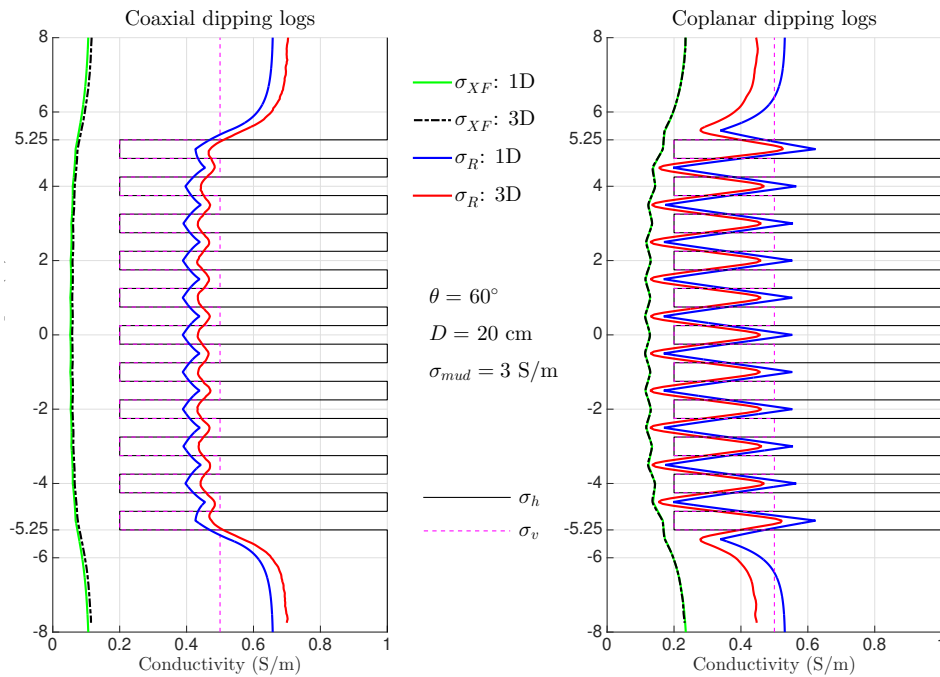


Figure 7: Comparison between logs without (1D) and with (3D) the influence of a borehole in a dipping well at  $60^\circ$  in a model composed of a sequence of isotropic sand laminae in an anisotropic shale host.

the dipping angle increases the borehole effect on the coaxial reactive (7.6% to 9.9%) and resistive (6.9% to 9.3%) signals, as compared to the vertical logs shown in figure 6. However, strong reductions are observed on the coplanar reactive (-0.7% to -0.02%) and resistive (-25.5% to -15.4%) signals.

Note that these percentage variations due to the borehole effect on the coplanar signals are practically the same as those of the isotropic shale laminae model (figure 5) whereas on the coaxial signals the borehole effect increases significantly on both the reactive (8.5% to 9.9%) and resistive (8.7% to 9.3%) components.

## CONCLUSION

The modeling results obtained in this comparative study reproduce some well-known characteristics of the coplanar logs with relation to coaxial logs as, for example, a greatest hornning effect in front of the interfaces, a strongest skin effect to the conductivity media, and a most prominent oscillation due to the laminae. In addition, the results show that the coplanar responses are more sensitive to the anisotropy and the borehole effects than the coaxial responses and that they have opposite behaviors with respect to the dipping angle, i.e., for small dip angles where the coaxial is least sensitive to these effects, the coplanar is most sensitive, and for large dip angles where the coaxial is most sensitive, the coplanar is least sensitive.

The main physical cause of these coaxial and coplanar opposite behaviors to the anisotropy and borehole effect is the same: the weight of the horizontal magnetic component of the horizontal dipole

( $TM_z$  mode contribution) on the coaxial and coplanar dipping logs, since this is the only one of the four magnetic field components that is sensitive to the anisotropy, and it is also the one subject to the strongest skin effect.

Although our 3D modeling code is able to simulate models with formation invasion zones, the study of the influence of the well on the data was performed only in models without invasion, because the comparison with 1D responses would not be possible otherwise. Therefore, this comparative analysis is extensive to data generated by the newer multicomponent configurations used in many EM-LWD tools, since they are obtained prior to the development of significant invasion zones.

As we were able to verify, the borehole exerts significant influence on the measured vertical and horizontal conductivities and hence on the estimated apparent anisotropy of the formation, especially when using conductive water-based muds. Thus, a quantitative assessment of this influence, as presented here, may be an important information to help the borehole effect corrections and consequently to improve the log interpretation.

## ACKNOWLEDGMENTS

The authors thank Petrobras for the support to this work through the research project number 2017/00424-6.



## REFERENCES

- Anderson, B., T. Barber, R. Bastia, J. B. Clauvaud, B. Coffin, M. Das, R. Hayden, T. Klimentos, C. C. Minh, and S. Williams, 2008, Triaxial induction – a new angle for an old measurement: *Oilfield Review*, **20**, 64–84.
- Anderson, B., S. Bonner, M. G. Lüling, and R. Rosenthal, 1992, Response of 2-MHz LWD resistivity and wireline induction tools in dipping beds and laminated formations: *The Log Analyst*, **33**, 461–475.
- Anderson, B. I., T. Barber, and T. M. Habashy, 2002, The interpretation and inversion of fully triaxial induction data; a sensitivity study: 43rd SPWLA Annual Logging Symposium, Oiso, Japan, Soc. Prof. Well Log. Analysts, Paper O.
- Bittar, M., H.-H. M. Wu, J. Ma, L. Pan, Y. Fan, M. Griffing, and C. Lozinsky, 2021, First LWD co-located antenna sensors for real-time anisotropy and dip angle determination, yielding better look-ahead detection: *Petrophysics - The SPWLA Journal of Formation Evaluation and Reservoir Description*, **62**, 296–310, doi: 10.30632/PJV62N3-2021a4.
- Carvalho, P. R. d., W. G. dos Santos, and C. Régis, 2010, Fundamentals of coaxial and coplanar coil arrays in induction tools: *Brazilian Journal of Geophysics*, **28**, 19–36, doi: 10.1590/S0102-261X2010000100002.
- Carvalho, P. R. d., C. R. T. Régis, and V. da Silva e Silva, 2018, Effects of the deviation angle of the borehole in the induction anisotropy logs: *Brazilian Journal of Geophysics*, **36**, 291–399, doi: 10.22564/rbgf.v36i4.1964.
- Clavaud, J.-B., R. Nelson, and U. K. Guru, 2005, Field example of enhanced hydrocarbon estimation in thinly laminated formation with a triaxial array induction tool: A laminated sand-shale analysis with anisotropic shale: SPWLA 46th Annual Logging Symposium, New Orleans, Louisiana, USA, Soc. Prof. Well Log. Analysts, Paper WW.
- Clegg, N., A. Duriez, V. Kiselev, S. Sinha, T. Parker, F. Jakobsen, E. Jakobsen, D. Marchant, and C. Schwarzbach, 2021, Detection of offset wells ahead of and around an LWD ultra-deep electromagnetic tool: Presented at the SPWLA 62nd Annual Logging Symposium, Virtual Event, Soc. Prof. Well Log. Analysts. doi: 10.30632/SPWLA-2021-0039.
- Gomes, R. M., P. S. Denicol, A. M. V. da Cunha, M. S. de Souza, B. F. Kriegshäuser, C. J. Payne, and A. Santos, 2002, Using multicomponent induction log data to enhance formation evaluation in deepwater reservoirs from Campus Basin, offshore Brazil: SPWLA 43rd Annual Logging Symposium, Oiso, Japan, Soc. Prof. Well Log. Analysts–SPWLA, Paper N.
- Jin, J.-M., 2015, *The finite element method in electromagnetics*, third ed.: Wiley, 800 pp.
- Kaufman, A. A., and G. Ytskovich, 2017, Basic principles of induction logging – Electromagnetic methods in borehole geophysics: Elsevier, 491 pp.
- Key, K., 2012, Is the fast hankel transform faster than quadrature?: *GEOPHYSICS*, **77**, F21–F30, doi: 10.1190/geo2011-0237.1.
- Kriegshäuser, B., O. Fanini, S. Forgang, G. Itskovich, M. Rabinovich, L. Tabarovsky, L. Yu, M. Epov, P. Gupta, and J. v. d. Horst, 2000, A new multicomponent induction logging tool to resolve anisotropic formations: Presented at the SPWLA 41st Annual Logging Symposium, Dallas, Texas, USA., Society of Petrophysicists and Well-Log Analysts.
- Moinfar, A., C. Torres-Verdin, R. K. Mallan, and R. Angeles, 2010, Time-lapse variations of multicomponent electrical resistivity measurements acquired in high-angle wells: *Petrophysics*, **51**, 408–427.
- Moran, J. H., and K. S. Kunz, 1962, Basic theory of induction logging and application to study of two-coil sondes: *GEOPHYSICS*, **27**, 829–858, doi: 10.1190/1.1439108.
- Omeragic, D., Z. Bayraktar, M. Thiel, T. Habashy, P. Wu, F. Shray, and V. H. G. Antezana, 2015, Triaxial induction interpretation in horizontal wells: Mapping boundaries, and characterizing anisotropy and fractures: SPWLA 56th Annual Logging Symposium, Long Beach, California, USA., Society of Petrophysicists and Well-Log Analysts, Paper I.
- Régis, C., P. R. de Carvalho, and V. da Silva e Silva, 2020, A new look at the causes of “polarization” horns in electromagnetic well logging: *GEOPHYSICS*, **85**, D233–D243, doi: 10.1190/geo2020-0163.1.
- Schenk, O., K. Gärtner, W. Fichtner, and A. Stricker, 2001, Pardiso: a high-performance serial and parallel sparse linear solver in semiconductor device simulation: *Future Generation Computer Systems*, **18**, 69 – 78, doi: 10.1016/S0167-739X(00)00076-5. (I. High Performance Numerical Methods and Applications. II. Performance Data Mining: Automated Diagnosis, Adaption, and Optimization).
- Si, H., 2015, Tetgen, a Delaunay-based quality tetrahedral mesh generator: *ACM Trans. Math. Softw.*, **41**, 1–36, doi: 10.1145/2629697.
- Ward, S. H., and G. W. Hohmann, 1987, Electromagnetic theory for geophysical applications, *in* Nabighian, M. N., ed., *Electromagnetic Methods in Applied Geophysics*, Vol. 1, Theory: SEG, volume 1 of *Investigations in Geophysics*, 130–311.
- Waxman, M., and L. Smits, 1968, Electrical Conductivities in Oil-Bearing Shaly Sands: *Society of Petroleum Engineers Journal*, **8**, 107–122, doi: 10.2118/1863-A.
- Zhang, Z., B. Yu, and C. Liu, 2012, Investigation of effects of large dielectric constants on triaxial induction logs: *Applied Mathematics*, **3**, 1811–1817, doi: 10.4236/am.2012.331246.

**Carvalho, P. R.; Régis, C.; Silva, V. S.:** All authors equally shared the tasks of code writing, discussion and interpretation of the results, and text revision.

Received on January 16, 2022 / Accepted on June 13, 2022



Creative Commons attribution-type CC BY